Nickel aluminide containing refractory-metal dispersoids 2: Microstructure and properties

T. Takahashi[a], D.C. Dunand[b]

[a]Department of Inorganic Materials, Hyogo Prefectural Institute of Industrial Research, Kobe 654, Japan
[b]Department of Materials Science and Engineering, Massachusetts Institute of Technology, Cambridge, MA 02139, USA

Abstract

NiAl containing 10 vol.% or 30 vol.% of molybdenum or tungsten was fabricated by hot isostatic pressing at 1000 °C or 1200 °C of powders synthesized by reactive mechanical alloying. The NiAl matrix exhibits sub-micron grains pinned by discrete refractory dispersoids with an average size between 55 nm and 110 nm. The two phases have negligible mutual solubility at room temperature, and the dispersoids exhibit only slight coarsening at the highest consolidation temperature. Dispersion-strengthening by the refractory second phase, measured by hardness indentation, is observed both at room temperature and at elevated temperature up to 700 °C, and increases with increasing volume fraction and decreasing size of the dispersoids. The oxidation resistance at 900 °C of NiAl containing 10 vol.% refractory-metal dispersoids is similar to that of unalloyed NiAl, indicating that the alumina scale protects the discontinuous refractory-metal dispersion within the NiAl matrix.

Keywords: Nickel; Aluminium; Refractory metals

1. Introduction

Stoichiometric NiAl exhibits a eutectic with many transition metals: vanadium, chromium, molybdenum, tungsten and rhenium [1-5]. The fine fibers or plates formed during directional solidification of these pseudo-binary systems lead to both strengthening and ductile-phase toughening [6-8]. These in-situ composites however suffer from weaknesses common to all directionally solidified eutectics [9], i.e. strong anisotropy of properties, slow fabrication rate (since the solidification must take place in a steep temperature gradient) and lack of flexibility for the volume fraction of reinforcement (since the composition of the melt must be near the eutectic composition of 10 at.% Mo and 1.4 at.% W, respectively [3,4]). Furthermore, since refractory-metal fibers form a continuous path into the materials, their oxidation is of concern at elevated temperatures.

The above issues can be resolved by incorporating discontinuous refractory-metal particulates in the NiAl matrix, e.g. by rapid solidification of the melt [10] or hot compaction of pre-alloyed NiAl and refractory-metal powders [11]. While the strength of these discontinuously reinforced composites is expected to be lower than that of NiAl reinforced with continuous fibers, they exhibit a creep rate at 1027 °C which is lower by two to three orders of magnitude than that of monolithic NiAl [11]. However, due to the large interparticle distance in these composites, the dominant mechanism is composite strengthening, which can be limited at temperatures where the matrix creeps readily [12,13], rather than dispersion strengthening, which can be very effective at these temperatures [14,15].

Mechanical alloying is a process by which a fine dispersion of insoluble particles can be formed in a matrix [16,17]. In a previous article [18], referred to in what follows as Part 1, we described the synthesis of powders of NiAl containing a sub-micron dispersion of molybdenum or tungsten by reactive mechanical alloying of elemental or intermetallic powders. In the present paper (Part 2), we report on the microstructure, hardness and oxidation behavior of the dispersion-strengthened materials formed by hot compaction of these mechanically alloyed powders.

2. Experimental procedures

Powders consisting of a NiAl matrix with a metal refractory dispersion were synthesized by reactive mechanical alloying for 20 h, as described in Part 1. Five compositions were examined: NiAl, NiAl–10vol.%Mo, NiAl–30vol.%Mo, NiAl–10vol.%W and NiAl–30vol.%W (Table 1), referred to in what follows as NiAl, NiAl–10Mo, NiAl–30Mo, NiAl–10W and NiAl–30W, respectively. Metallic powders were purchased from Mitsuwata Chemical Co.: 99.5%-pure aluminum with average size 150 μm, 99.9%-pure nickel with average size 5.5 μm, 99.9%-pure molybdenum with average size 2.3 μm, and 99%-pure tungsten with about the same average size. Before use, the nickel, molybdenum and tungsten were annealed for 1 h in hydrogen at 500 °C, 700 °C and 900 °C, respectively, to reduce any oxide present at the surface of the powders. Scanning electron microscope images show that the nickel powder surface has a spiky appearance, while that of the other powders is smooth. For the powders produced by the intermetallic route described in Part 1 — whereby the intermetallic precursor NiMo is first synthesized by hydrogen reduction, before being mechanically alloyed to metal powders to form NiAl containing a molybdenum dispersion — the oxide powders were purchased from Wako Pure Chemical Industries Co.: SEM images indicate that NiO is in the form of 5-μm equiaxed particles and 99.5%-pure MoO$_3$ is in the form of platelets, about 4 μm in length and 1 μm thick. In what follows, we refer to all samples mechanically alloyed by the metal route without further labeling, but specifically mention the intermetallic route for the appropriate samples.

After 20 h of mechanical alloying, the powders were annealed for 1 h at 1000 °C under vacuum and subsequently densified by Hot Isostatic Pressing (HIP) for 1 h at 1000 °C or 1200 °C under a pressure of 200 MPa. Thin foils of the HIPed specimens were prepared by ion-milling and examined by transmission electron microscopy (TEM) with a JEOL Model 2000 FX at a voltage of 200 kV.

Room-temperature micro-Vickers hardness measurements were performed on HIPed samples with a diamond indenter under a load of 100 gf. Micro-Vickers hardness at elevated temperature was measured with a sapphire indenter under a load of 200 gf in vacuum. Finally, cuboid specimens were cut from HIPed samples and subjected to isothermal oxidation at 900 °C with dry air flowing at a rate of 10 l h^{-1} in a Seiko thermogravimeter (Model TG-DTA 320).

3. Results

Fig. 1 shows the microstructure of refractory-free NiAl: while large grains were observed in other micrographs of this sample, a few sub-micron grains are visible in Fig. 1. Figs. 2 and 3 are TEM images of HIPed samples of NiAl–10Mo and NiAl–30 Mo, respectively, showing molybdenum dispersoids located both within NiAl grains and at grain boundaries. In Fig. 4, corresponding to NiAl–10Mo HIPed at the higher temperature of 1200 °C, the dispersoids are noticeably larger than for the corresponding sample HIPed at

Table 1
Chemical composition and theoretical density of samples

Sample	Ni (wt.%)	Al (wt.%)	Refractory (wt.%)	Theoretical density (g cm^{-3})
NiAl	68.6	31.4	—	5.9
NiAl–10Mo	57.5	26.5	16.0Mo	6.3
NiAl–30Mo	39.5	18.1	42.4Mo	7.2
NiAl–10W	50.4	23.1	26.5W	7.2
NiAl–30W	28.7	13.2	58.2W	9.9

Fig. 1. TEM image of NiAl HIPed at 1000 °C.

1000 °C (Fig. 2). On the other hand, NiAl–10Mo processed by the intermetallic route (Fig. 5) displays smaller dispersoids than when processed by the metal route (Fig. 2). Figs. 6 and 7 show the structure of NiAl–10W after HIPing at 1000 °C and 1200 °C, respectively. Grain size and dispersoid size for some of the samples containing 10 vol.% refractory metal are listed in Table 2. Fig. 8 corresponds to NiAl–30W after HIPing at 1000 °C.

In Fig. 9, the room-temperature hardness is plotted as a function of the dispersoid content for different HIPing temperature: hardness increases with increasing dispersoid content and decreasing HIPing temperature. One data point for NiAl–10Mo is given for a sample from powders prepared by the oxide route and HIPed at 1200 °C, which exhibits a higher hardness ($H_V = 414$) than the corresponding sample prepared by the metal route ($H_V = 388$).

Figs. 10(a) and 10(b) show hardness as a function of temperature for the molybdenum- and tungsten-containing samples, respectively. The dispersion-strengthened samples show markedly higher hardness than the dispersion-free metals up to 700 °C.

The thermogravimetric curves for samples NiAl, NiAl–10Mo and NiAl–10W are plotted in Fig. 11, and show a parabolic mass gain as a result of oxidation. The presence of refractory metal in NiAl does not significantly alter the oxidation kinetics.

4. Discussion

4.1. Microstructure

Fig. 1 for NiAl without refractory shows that the material has a fine grain structure, with some grains about 0.5 μm in diameter. Much larger grains spanning the field of view were also observed, thus preventing determination of the average grain size from TEM images. Since the material was HIPed at 1000 °C, a temperature at which grain growth is expected, the presence of sub-micron grains can only be explained by a fine dispersion pinning the grain boundaries. A few small dispersoids are indeed visible in Fig. 1, and are most probably alumina resulting from contamination during the mechanical alloying step. Room-temperature hardness ($H_V = 366$) is however close to that measured on a large NiAl powder particle fabricated by melt solidification ($H_V = 348$), indicating that the oxide content is not sufficient to induce significant Orowan strengthening.

Electron diffraction of a dispersoid about 90 nm in size, extracted from sample NiAl–10Mo, showed the lattice spacing of pure molybdenum. This was confirmed by X-ray diffraction of the dispersoid, which

exhibited the main molybdenum peak but none of the peaks corresponding to nickel or aluminum. Conversely, the matrix showed aluminum and nickel peaks but no molybdenum peaks. The first observation is in agreement with Subramanian et al. [19], who measured very low values for the solubility of molybdenum in NiAl (0.1 ± 0.1 at.%) for directionally solidified samples annealed between 1200 °C and 1500 °C. However, they reported up to 18 at.% nickel and aluminum within the molybdenum phase, in disagreement with both our findings and those of Ref. [3], giving a solubility of 1 at.% Al and 1.5 at.% Ni in molybdenum at 1600 °C. The same experiment was performed on an extracted tungsten dispersoid from sample NiAl–10W, leading to similar results, i.e. the two phases show no measurable mutual solubility. This is in agreement with Nash [20] who reported a value of about 0.2 at.% for the solubility of tungsten in NiAl, and with Locci et al. [10], who found tungsten precipitates in rapidly solidified NiAl–0.5at.%W.

As shown in Fig. 2, NiAl–10Mo consists of a matrix with grain size $D = 370$ nm, containing well-dispersed, equiaxed molybdenum dispersoids with average diameter $d = 90$ nm. These observations are in agreement with those of Hwang et al. [21], who used reactive mechanical alloying in an attritor mill to synthesize

Fig. 2. TEM image of NiAl–10Mo HIPed at 1000 °C. Some molybdenum dispersoids are marked with arrows.

NiAl from elemental powders with additions of 5 at.% Mo, 2.7 at.% Ti and 2.6 at.% O. After extrusion at 1127 °C, they observed a microstructure consisting of fine-grained NiAl containing both oxide particles and molybdenum dispersoids with sizes between 10 nm and 100 nm, mostly located at NiAl grain boundaries.

Figs. 2-5 also show that the larger molybdenum dispersoids are typically located at NiAl grain boundaries, and that these dispersoids exhibit cusps at the intersection with the grain boundaries, indicating that the interfacial energy is an important contribution to the equilibrium shape of the particles. Molybdenum dispersoids less than the average size are typically located within grains and have near-spherical shape. Both shapes indicate that some diffusion took place during the high-temperature treatment, since mechanically alloyed molybdenum dispersoids show flattened shapes, as reported in Part 1.

Sample NiAl-30 Mo (Fig. 3) exhibits dispersoids with a similar size as for sample NiAl-10 Mo; however, dispersoid overlap prevented the quantitative determination of the dispersoid size and grain size. Some agglomeration of the dispersoid is also visible in Fig. 3, since the percolation limit is exceeded.

Sample NiAl-10Mo, which was HIPed at 1200 °C, Fig. 4, exhibits a larger average dispersoid size ($d = 110$

nm) than the equivalent sample HIPed at 1000 °C ($d = 90$ nm), Fig. 2. Coarsening is however modest, as a result of the low solubility of molybdenum in NiAl reported above. This observation is in agreement with Subramanian et al. [19], who found that molybdenum fibers in a directionally solidified NiAl-Mo composite coarsened slowly at 1200 °C. However, the latter material is expected to have significantly coarser grains than the mechanically alloyed materials in the present study, for which accelerated coarsening by grain-boundary diffusion may possibly take place.

Fig. 5 illustrates that the dispersoid size ($d = 60$ nm) for NiAl-10Mo produced by the intermetallic route and HIPed at 1000 °C is significantly smaller than for the equivalent sample produced by the metal route ($d = 90$ nm): this is expected, since, as shown in Part 1, powder fragmentation is more efficient by the intermetallic route, as a result of the brittle nature of the intermetallic reactant used during mechanical alloying.

As shown in Fig. 6, NiAl-10W exhibits finer dispersoids ($d = 55$ nm) than the equivalent molybdenum-containing sample ($d = 90$ nm). Fig. 6 also shows some elongated dispersoids, similar to the flattened tungsten particles observed in Part 1 in the mechanically alloyed powders, which resulted from plastic deformation of the powder upon impact during
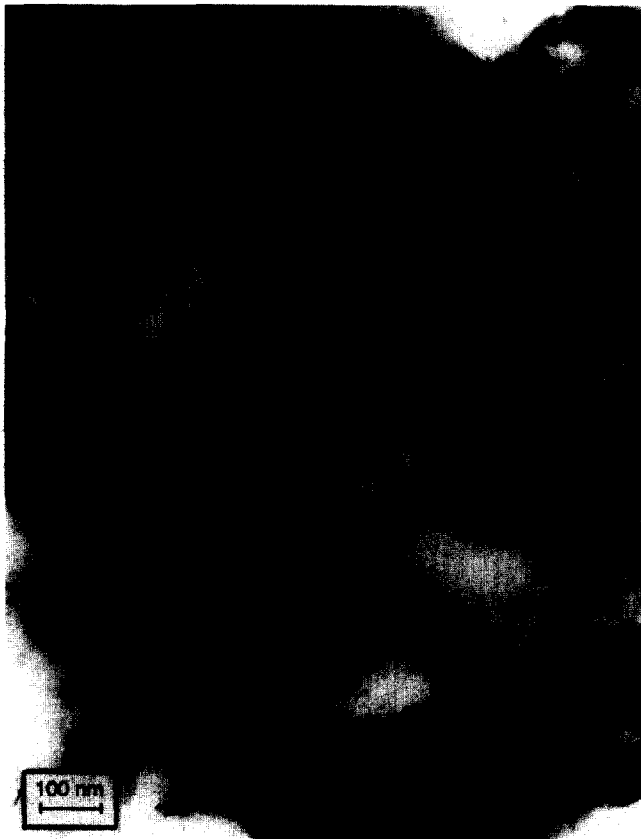

Fig. 3. TEM image of NiAl-30Mo HIPed at 1000 °C.

Fig. 4. TEM image of NiAl-10Mo HIPed at 1200 °C.

Fig. 5. TEM image of NiAl–10Mo synthesized by the intermetallic route and HIPed at 1000 °C.
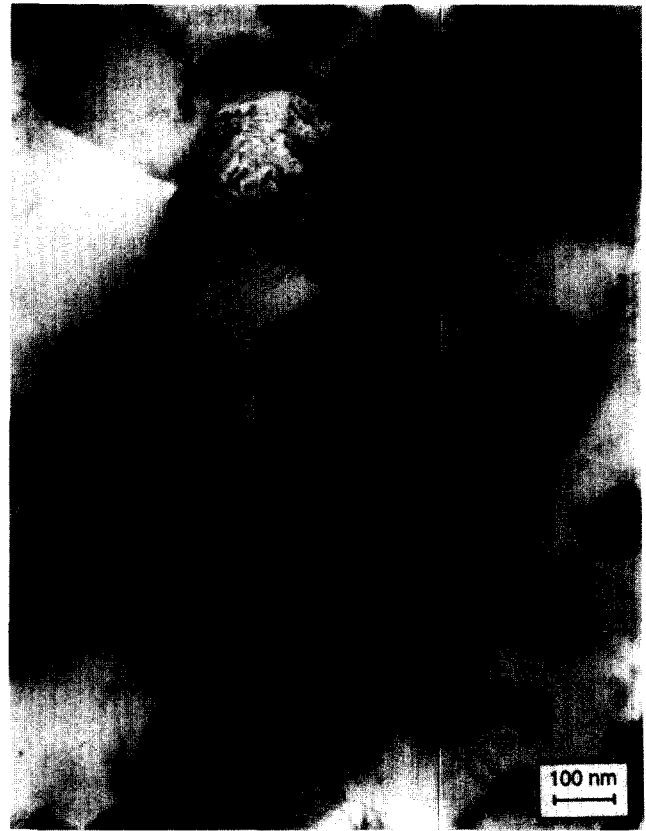

Fig. 6. TEM image of NiAl–10W HIPed at 1000 °C.

milling. The smaller size and non-equilibrium shape of the tungsten dispersoids both indicate that they coarsened less than the molybdenum dispersoids during HIPing, possibly as a result of a lower diffusivity due to the higher melting point of tungsten. Indeed, Vedula et al. [11] found no measurable coarsening of tungsten in NiAl after annealing for 175 h at 1250 °C. Fig. 7 however shows that all tungsten dispersoids are equiaxed after HIPing at 1200 °C, indicating that significant diffusion took place at this temperature. Finally, Fig. 8 shows that the NiAl–30W sample contains dispersoids with a diameter comparable to that of NiAl–10W; overlap did not allow a quantitative determination.

Zener's equation for the limiting grain size D of a matrix containing dispersoids of radius r and volume fraction f

$$D = \frac{4r}{3f} \tag{1}$$

predicts for NiAl–10Mo and NiAl–10W grain sizes between 370 nm and 600 nm, in rough agreement with grain sizes measured on TEM images (Table 2). The above estimates, together with the location of the dispersoids at grain boundaries, indicate that NiAl

grains are pinned by the dispersoids, since grain growth is expected at 1000 °C, corresponding to a homologous temperature of 0.67 for NiAl. Locci et al. [10] also found that, in NiAl–0.5at.%W produced by rapid solidification, tungsten precipitates were effective at limiting the size of the grains after annealing at 1000 °C and 1300 °C; unalloyed NiAl however exhibited grain growth.

4.2. Hardness

Fig. 9 shows that significant strengthening results from the refractory dispersoids at room temperature, as expected from Orowan strengthening $\Delta\sigma$ for unshearable dispersoids

$$\Delta\sigma = M \frac{0.4\,Gb}{\pi L} \frac{\ln(\bar{d}/b)}{\sqrt{1-\nu}} \tag{2}$$

where G is the single-crystal shear modulus, ν is Poisson's ratio, b is the Burger's vector, M is the mean orientation factor, and $\bar{d} = (2/3)^{1/2}d$ is the mean diameter of a circular section in a random plane for a sphere of diameter d. The dispersoid separation is $L = \bar{d}\{[\pi/(4V_p)]^{1/2} - 1\}$ for a cubic arrangement of spherical dispersoids of volume fraction V_p [22].

Eq. (2) predicts a yield stress increment $\Delta\sigma = 414$ MPa for NiAl–10Mo, large when compared to the yield strength of about 100 MPa for stoichiometric NiAl [23]. If the particles are sheared, a lower strengthening level is expected: TEM observation of deformed samples is however necessary to determine which mechanism is operational. We note that Hall–Petch strengthening is negligible for stoichiometric NiAl,

since the Hall–Petch slope is near zero (as measured for grain sizes between 10 μm and 300 μm [23]), but may further contribute to strengthening for off-stoichiometric compositions, for which the slope is positive [23].

Figs. 10(a) and 10(b) show that the refractory-containing NiAl is harder than either unalloyed NiAl or the unalloyed refractory metal up to 700 °C, indicating that dispersion strengthening is effective at elevated temperatures as well. The hardness of the unalloyed

Fig. 7. TEM image of NiAl–10W HIPed at 1200 °C.

Fig. 8. TEM image of NiAl–30W HIPed at 1000 °C.

Table 2
Room-temperature micro-Vickers hardness, measured
dispersoid diameter, measured grain size and predicted grain size (Eq. (1)) for samples containing 10 vol.% dispersoids

Sample	HIP temperature (°C)	HV at 25 °C	Dispersoid diameter (nm)	Observed grain size (nm)	Predicted grain size (nm)
NiAl–10Mo	1000	422	90	370	600
NiAl–10Mo	1200	388	110	—[b]	730
NiAl–10Mo[a]	1000	—	60	470	400
NiAl–10W	1000	498	55	250	370

[a]Intermetallic route.
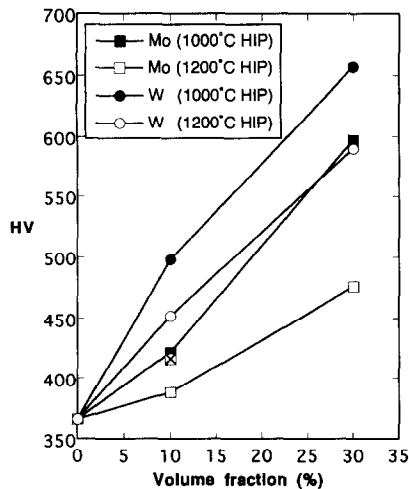[b]Too large to measure on TEM micrographs.

Fig. 9. Room-temperature Vickers microhardness as a function of refractory content for mechanically alloyed powders (metal route) HIPed at 1000 °C and 1200 °C. Crossed data point corresponds to sample fabricated from powders mechanically alloyed by the intermetallic route.

NiAl decreases gradually with increasing temperature. Since coarsening of the dispersoids is negligible at this temperature (Table 2), weakening of the matrix above about 500 °C, corresponding to the ductile-to-brittle transition temperature of NiAl [23,24], is probably responsible for the drop in hardness. The refractory-containing materials thus consist of a ductile matrix containing ductile dispersoid, similar to γ/γ' nickel-base superalloys, which also exhibit strength and creep resistance superior to either of their phases. Figs. 9 and 10 also show that tungsten is more effective than molybdenum for strengthening NiAl. This may be due to the higher strength of tungsten (if the dispersoids are sheared upon deformation), or to the finer size of the tungsten dispersoids, Table 2, (effective for dislocation bowing, Eq. (2)) as a result of better fragmentation during mechanical alloying, or lesser coarsening at elevated temperature. The hardness difference between the two systems is however small, and, in terms of density-compensated hardness (Table 1), molybdenum ($\rho = 10.2$ g cm^{-3}) is more effective than tungsten ($\rho = 19.3$ g cm^{-3}) for short-term strengthening of NiAl.

4.3. Oxidative stability

Fig. 11 indicates that oxidation at 900 °C of the refractory-containing alloys decreases with time and is similar to that of unalloyed NiAl: after 4 h isothermal holding, the mass gain for all samples is only 0.10–0.19%. This is in contrast with the results reported in Part 1 for the oxidation of loose powders, for which rapid oxidation of the refractory phase was
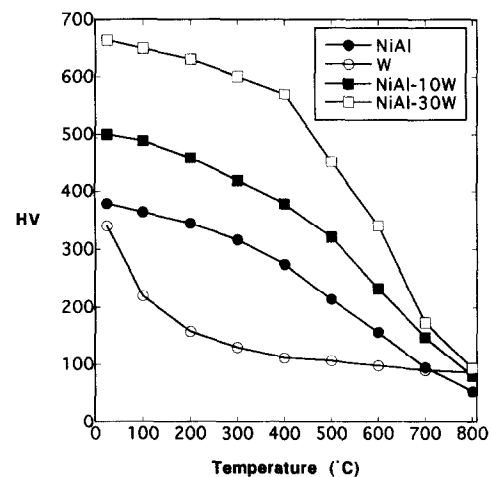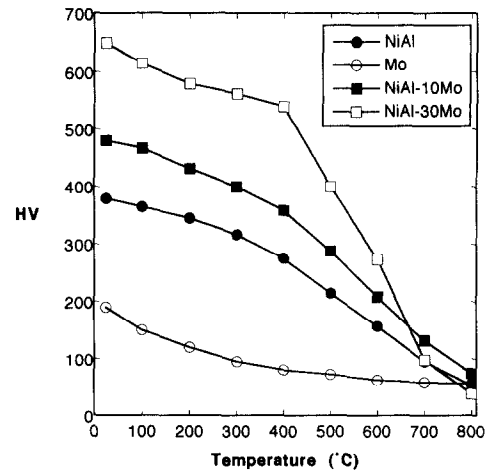

Fig. 10. Vickers microhardness as a function of temperature, from Ref. [28]: (a) NiAl, NiAl-10Mo, NiAl-30Mo and recrystallized molybdenum; (b) NiAl, NiAl-10W, NiAl-30W and annealed tungsten.
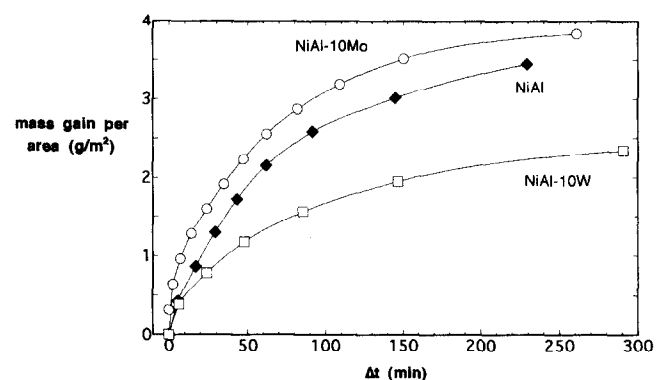

Fig. 11. Thermogravimetric curves for NiAl, NiAl-10Mo and NiAl-10W isothermally oxidized at 900 °C in flowing air.

observed at this temperature, as a result of the high surface-to-volume ratio of the powders and the high oxidation tendency of both refractory metals. Power-law fitting of the curves in Fig. 11 gives exponents

$n = 0.59$ for NiAl, $n = 0.41$ for NiAl-10Mo and $n = 0.50$ for NiAl-10W, i.e. close to the value $n = 0.5$ expected for parabolic growth behavior of the oxide. We conclude that the refractory phase in NiAl does not prevent the formation of the tenacious oxide layer [23], which then protects the refractory from oxidation. We note that directionally solidified eutectics with a similar volume fraction of refractory-metal fibers are expected to be less oxidation-resistant, since, unlike the dispersoids in the alloys investigated in the present paper, continuous fibers form an uninterrupted path for oxidation. While preliminary in nature, these results indicate that these refractory-dispersion-strengthened alloys may be used at 900 °C without coatings, similarly to unalloyed NiAl alloys.

4.4. Alloy system

The goal of the present investigation is to strengthen a low-density, oxidation-resistant, high-melting, intermetallic matrix (β-NiAl) with a fine dispersion of thermodynamically stable refractory metal (α-Mo or α-W) exhibiting high strength, high ductility and low coarsening kinetics at elevated temperature. The α/β structure emulates to a certain extent the γ/γ' Ni-Ni$_3$Al combination found in nickel-base superalloys, with the important difference that the α-dispersoids are disordered, while the β-matrix is ordered. Three of the four α/β alloys exhibit significantly lower densities (Table 1) than typical γ/γ' superalloys ($\rho = 8400$ kg m^{-3}): NiAl-10Mo is 25% lighter, NiAl-30Mo and NiAl-10W are 14% lighter, while NiAl-30W is 18% heavier. Density is a critical property in rotating components subjected to "centrifugal" stresses: a 9% decrease of density from 8650 kg m^{-3} to 7860 kg m^{-3} was calculated to lead to a 300% increase in life for a turbine disk [25], all other properties being equal.

While refractory-metal dispersoids are not as light, insoluble and oxidation-resistant as ceramic dispersoids, they have the following advantages: ductility at or near room temperature (possibly increasing the toughness of the material, since molybdenum is not embrittled by NiAl [8]), ductility at high temperature (thus forming a ductile–ductile α/β system similar to the γ/γ' superalloys) and high thermal conductivity (which is important for cooled structures).

A further effect of the high volume fraction of dispersoids is the stabilization of sub-micron grains (Table 2): as the grain size decreases, NiAl has been shown to exhibit improved ductility and toughness as well as lower brittle-to-ductile transition temperature [23,24]. This was recently confirmed for extruded NiAl with sub-micron grains pinned by oxide dispersoids

fabricated by mechanical alloying: Dymek et al. [26] reported a significant increase in room-temperature compressive ductility as compared to cast, coarse-grained NiAl. They note that, owing to texture, the general requirements for polycrystalline ductility are met (five independent slip systems). Finally, the presence of stable, sub-micron grains and dispersoids opens the possibility of superplasticity in these materials [27].

In summary, this paper is an exploratory study of novel refractory-dispersion-strengthened intermetallics. While the results presented above show encouraging strengthening levels and high oxidation resistance, further work is needed to assess other critical properties (e.g. tensile strength, ductility, toughness, creep-, fatigue- and corrosion-resistance, etc.) before these dispersion-strengthened α/β alloys can be considered for structural applications at elevated temperature.

5. Conclusions

- NiAl powders containing high volume fractions (10 vol.% or 30 vol.%) of finely dispersed refractory metals (molybdenum or tungsten), synthesized by reactive mechanical alloying of elemental powders, were consolidated by hot isostatic pressing at 1000 °C or 1200 °C.

- Consolidated specimens exhibit a NiAl matrix with sub-micron grains pinned by discrete molybdenum or tungsten dispersoids with an average size between 55 nm and 110 nm. The matrix and refractory-metal dispersoids exhibit no mutual solubility at room temperature, after exposure for 2 h at 1000 °C.

- Room-temperature hardness increases with increasing refractory-metal content, as a result of dispersion strengthening, and decreases with increasing processing temperature, as a result of coarsening of the refractory dispersoids.

- Up to 700 °C, hardness for all refractory-containing samples is higher than either unalloyed NiAl or the respective unalloyed refractory metal, indicating that dispersion-strengthening is active at temperatures where both phases are ductile.

- Thermogravimetric experiments at 900 °C show that the oxidation resistance of NiAl containing 10 vol.% refractory-metal dispersoids is as good as that of unalloyed NiAl: the NiAl matrix protects the oxidation-prone refractory-metal dispersion because the refractory phase does not form a continuous path in the matrix.

Acknowledgments

References

[1] F.H. Hayes, P. Rogl and E. Schmidt, in G. Petzow and G. Effenberg (eds.), Ternary Alloys, Vol. 8, VCH, New York, 1993, p. 40.

[2] P. Rogl, in G. Petzow and G. Effenberg (eds.), Ternary Alloys, Vol. 4, VCH, New York, 1991, p. 400.

[3] O. Kubaschewski, in G. Petzow and G. Effenberg (eds.), Ternary Alloys, Vol. 7, VCH, New York, 1993, p. 199.

[4] Z.M. Alekseeva, in G. Petzow and G. Effenberg (eds.), Ternary Alloys, Vol. 8, VCH, New York, 1993, p. 49.

[5] J.G. Webber and D.C. Van Aken, Scr. Metall. Mater., 23 (1989) 193.

[6] M.Y. He, F.E. Heredia, D.J. Wissuchek, M.C. Shaw and A.G. Evans, Acta Metall. Mater., 41 (1993) 122.

[7] K.S. Ravichandran, Scr. Metall. Mater., 26 (1992) 1389.

[8] F.E. Heredia, M.Y. He, G.E. Lucas, A.G. Evans, H.E. Deve and D. Konitzer, Acta Metall. Mater., 41 (1993) 505.

[9] M. McLean, Directionally Solidified Materials for High Temperature Service, The Metals Society, London, 1983.

[10] I.E. Locci, R.D. Noebe, J.A. Moser, D.S. Lee and M. Nathal, in C.T. Liu, A.I. Taub, N.S. Stoloff and C.C. Koch (eds), High-Temperature Ordered Intermetallic Alloys III, MRS, Pittsburgh, PA, 1988, p. 639.

[11] K. Vedula, V. Pathare, I. Aslanadis and R.H. Titran, in C.C. Koch, C.T. Liu and N.S. Stoloff (eds), High-Temperature Ordered Intermetallic Alloys, MRS, Pittsburgh, PA, 1984, p. 411.

[12] J.W. Hutchinson and R.M. McMeeking, in S. Suresh, A. Mortensen and A. Needleman (eds.), Fundamentals of Metal Matrix Composites, Butterworth, Boston, 1993, p. 158.

[13] D.C. Dunand and B. Derby, in S. Suresh, A. Mortensen and A. Needleman (eds.), Fundamentals of Metal Matrix Composite, Butterworth, Boston, 1993, p. 191.

[14] J.-P. Poirier, Creep of Crystals, Cambridge University Press, Cambridge, 1985.

[15] J. Cadek, Creep in Metallic Materials, Elsevier, Amsterdam, 1988.

[16] C.C. Koch, Ann. Rev. Mater. Sci., 19 (1989) 121.

[17] P.S. Gilman and K.K. Sankaran, in Y.-W. Kim and W.M. Griffith (eds), Symposium on Dispersion Strengthened Aluminum Alloys, The Minerals, Metals and Materials Society, 1988, p. 631.

[18] T. Takahashi and D.C. Dunand, Mater. Sci. Eng., 192/193 (1995) 186-194.

[19] P.R. Subramanian, M.G. Mendiratta, D.B. Miracle and D.M. Dimiduk, in D.L. Anton, P.L. Martin, D.B. Miracle and R. McMeeking (eds.), Intermetallic Matrix Composites, MRS, Pittsburgh, PA, 1990, p. 147.

[20] P. Nash, in C.C. Koch, C.T. Liu and N.S. Stoloff (eds.), High-Temperature Ordered Intermetallic Alloys, MRS, Pittsburgh, PA, 1984, p. 423.

[21] S.J. Hwang, P. Nash, M. Dollar and S. Dymek, in L.A. Johnson, D.P. Pope and J.O. Stiegler (eds), High-Temperature Ordered Intermetallic Alloys IV, MRS, Pittsburgh, PA, 1990, p. 661.

[22] L.M. Brown and R.K. Ham, in A. Kelly and R.B. Nicholson (eds.), Strengthening Methods in Crystals, Elsevier, Amsterdam, 1971, p. 9.

[23] R.D. Noebe, R.R. Bowman and M.V. Nathal, Intern. Mater. Rev., 38 (1993) 193.

[24] D.B. Miracle, Acta Metall. Mater., 41 (1993) 649.

[25] R.W. Fawley, in C.T. Sims and W.C. Hagel (eds.), The Superalloys, Wiley, New York, 1972, p. 3.

[26] S. Dymek, M. Dollar, S.J. Hwang and P. Nash, Mater. Sci. Eng., A152 (1992) 160.

[27] O.A. Kaibyshev, Superplasticity of Alloys, Intermetallides and Ceramics, Springer-Verlag, Berlin, 1992.

[28] Metals Handbook: Properties and Selection: Nonferrous Alloys and Pure Metals, ASM, Metals Park, OH, 1979.